1

Spectroscopic Ellipsometry: Basic Principles

1.1 Spectroscopic Ellipsometry

Spectroscopic ellipsometry measures the change of light polarization upon its reflection from the sample. A schematic diagram of the experimental setup is displayed in Figure 1.1. The detector of spectroscopic ellipsometry measures the quantities Ψ and Δ at each corresponding wavelength/photon energy. Parameter Ψ denotes the ratio of the amplitude of p- to s-polarized reflected light, while Δ their phase difference. Specifically, p-polarized light has the electric field vector parallel to the plane of incidence, while s-polarized light consists of the electric field vector perpendicular to the incident plane (Figure 1.2).

Typically, the energy range that is commonly used for spectroscopic ellipsometry measurement is the ultraviolet–visible (UV–vis) regime (~0.5–6 eV). In this range, sample properties such as the optical band structures and bandgaps can be investigated. Nevertheless, other regions of the electromagnetic spectrum have also been used in spectroscopic ellipsometry measurements. For instance, the use of mid-to-near-infrared range spectroscopic ellipsometry in the study of low-energy structures in 1T′-phase two-dimensional transition metal dichalcogenides (2D-TMDs), such as their fundamental gap and the anisotropic plasmons, will be discussed in Section 3.4 of Chapter 3.

While spectroscopic ellipsometry is a fast, nondestructive, and surface-sensitive (down to a few angstroms) optical characterization technique, the mathematical analysis involved in extracting the optical parameters from the raw (Ψ, Δ) data is not a straightforward process (see Section 1.5 and Figure 1.7). Generally, to analytically elucidate the optical parameters from the raw (Ψ, Δ) data, the sample in consideration must be homogenous, isotropic, and of sufficient thickness. In more general cases, complications will arise and optical models with associated numerical approximation techniques are required for the proper elucidation of meaningful optical results.

Introduction to Spectroscopic Ellipsometry of Thin Film Materials: Instrumentation, Data Analysis, and Applications, First Edition. Andrew T. S. Wee, Xinmao Yin, and Chi Sin Tang.

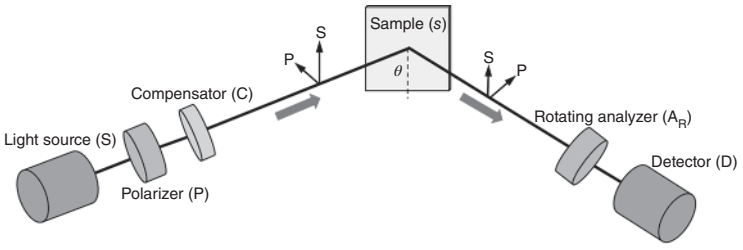

Figure 1.1 Schematic diagram of spectroscopic ellipsometry with the rotating-analyzer configuration.

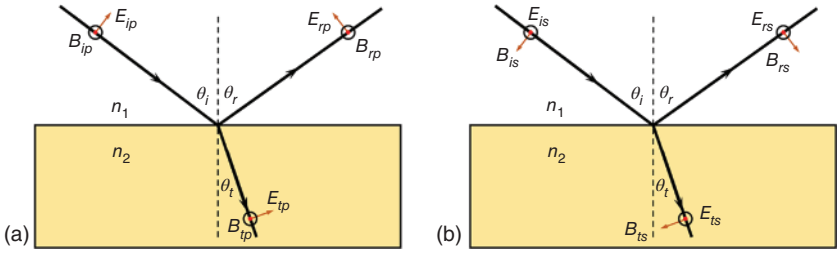

Figure 1.2 Electric and magnetic fields for (a) p-polarized and (b) s-polarized waves [1].

1.1.1 p- and s-Polarized Lights and Fresnel Coefficients

The electromagnetic wave features of light can be expressed in terms of its electric, E, and magnetic field, B, components [1]:

$$\vec{E}(\vec{r},t) = \vec{E}_0 \exp[i(\vec{k}\cdot\vec{r} - \omega t + \delta)] \tag{1.1}$$

$$\vec{B}(\vec{r},t) = \vec{B}_0 \exp[i(\vec{k}\cdot\vec{r} - \omega t + \delta)] \tag{1.2}$$

where $\vec{k}$ denotes the wave vector, ω denotes the angular frequency, and δ denotes the initial phase.

When light is reflected or transmitted through a sample/medium via an oblique angle, the electromagnetic wave can be resolved into two components – p-polarized (in-plane incidence) and s-polarized (perpendicular to incident plane) E-field components, respectively.

For a medium with refractive index n, based on Maxwell's equations and boundary conditions, the amplitude of the reflection coefficient for the p-polarized light is expressed as

$$r_p \equiv \frac{E_{rp}}{E_{ip}} = \frac{n_{\{t\}}\cos\theta_i - n_i\cos\theta_t}{n_t\cos\theta_i + n_i\cos\theta_t} \tag{1.3}$$

Likewise, the amplitude of the transmission coefficient for the p-polarized light can be expressed as

$$t_p \equiv \frac{E_{tp}}{E_{ip}} = \frac{2n_i\cos\theta_i}{n_t\cos\theta_i + n_i\cos\theta_t} \tag{1.4}$$

whereas the s-polarized counterparts are expressed as

$$r_s \equiv \frac{E_{rs}}{E_{is}} = \frac{(n_i \cos\theta_i - n_t \cos\theta_t)}{(n_i \cos\theta_i + n_t \cos\theta_t)} \tag{1.5a}$$

$$r_p \equiv \frac{E_{ts}}{E_{is}} = \frac{2n_i \cos\theta_i}{n_i \cos\theta_i + n_t \cos\theta_t} \tag{1.5b}$$

These equations are known as the Fresnel equations. When the refractive indices are complex, $\widetilde{n}$, the Fresnel equations still hold. The complex dielectric function can be obtained via the expression

$$\widetilde{n}^2 \equiv \varepsilon \tag{1.6}$$

Based on Snell's law, the Fresnel equations for reflection can be further generalized as

$$r_{\mathrm{p}} = \frac{\widetilde{n}_{ti}^2 \cos\theta_i - \left(\widetilde{n}_{ti}^2 - \sin^2\theta_i\right)^{\frac{1}{2}}}{\widetilde{n}_{ti}^2 \cos\theta_i + \left(\widetilde{n}_{ti}^2 - \sin^2\theta_i\right)^{\frac{1}{2}}} \tag{1.7a}$$

$$r_{\mathrm{s}} = \frac{\cos\theta_i - \left(\widetilde{n}_{ti}^2 - \sin^2\theta_i\right)^{\frac{1}{2}}}{\cos\theta_i + \left(\widetilde{n}_{ti}^2 - \sin^2\theta_i\right)^{\frac{1}{2}}} \tag{1.7b}$$

where $\widetilde{n}$ denotes the complex refractive index and

$$\widetilde{n}_{ti} = \frac{\widetilde{n}_t}{\widetilde{n}_i} \tag{1.8}$$

The reflectances of the p- and s-polarized lights are expressed by

$$R_{\mathrm{p}} \equiv \frac{I_{rp}}{I_{ip}} = \left|\frac{E_{rp}}{E_{ip}}\right|^2 = |r_{\mathrm{p}}^2| \tag{1.9a}$$

$$R_{\mathrm{s}} \equiv \frac{I_{rs}}{I_{is}} = \left|\frac{E_{rs}}{E_{is}}\right|^2 = |r_{\mathrm{s}}^2| \tag{1.9b}$$

where the light intensity $I = n|E|^2$. Since the difference between r_{p} and r_{s} is maximized at the Brewster angle [2], ellipsometric measurements are usually performed at incident angles, θ_i, typically in the range of 70–80° for the optical characterization of semiconducting systems [3].

In multilayered systems, the resultant amplitude of the reflection coefficients is expressed as the sum of individual components of the reflection and transmission coefficients at each interface. The phase differences of each wave are considered in the analysis.

1.1.2 Representation of Polarized Lights

Electromagnetic waves traversing along the z-direction can be expressed by superimposing two waves that are oscillating parallel to the x- and y-axes. The vector sum of the respective E-fields, E_x and E_y, is given by

$$E(z,t) = E_x(z,t) + E_y(z,t)$$
$$= E_{x_0} \exp i(\omega t - kz + \delta_x)\hat{x} + E_{y_0} \exp i(\omega t - kz + \delta_y)\hat{y} \tag{1.10}$$

where $\hat{x}$ and $\hat{y}$ denote the unit vectors along the respective axes. Ultimately, the phase difference, $\delta_y - \delta_x$, is the most important quantity that determines the state of the polarization of the resultant wave.

To mathematically represent the polarization states and analyze the effects of the optical components in a neat and elegant manner, they are expressed in the form of *Jones vectors* and *Jones matrices* [4].

A complete representation of the polarization of a wave can be expressed in the form of the Jones vector as

$$E(z,t) = \begin{bmatrix} E_{x_0} \exp i\delta_x \\ E_{y_0} \exp\ i\delta_y \end{bmatrix} \tag{1.11}$$

which can be further simplified as

$$E(z,t) = \begin{bmatrix} E_x \\ E_y \end{bmatrix} \tag{1.12}$$

where $E_x = E_{x_0} \exp i\delta_x$ and $E_y = E_{y_0} \exp i\delta_y$.

Relative changes to the amplitude and phase are important in spectroscopic ellipsometry. Jones vectors are therefore expressed in terms of normalized intensities. Linearly polarized waves along the x- and y-axes are expressed, respectively, as

$$E_{\text{lin},x} = \begin{bmatrix} 1 \\ 0 \end{bmatrix} \qquad E_{\text{lin},y} = \begin{bmatrix} 0 \\ 1 \end{bmatrix} \tag{1.13}$$

When light is linearly polarized at an orientation of 45°,

$$E_{+45^\circ} = \frac{1}{\sqrt{2}} \begin{bmatrix} 1 \\ 1 \end{bmatrix} \tag{1.14}$$

In the formalism where optical components are expressed in the form of 2×2 matrices, they are known as *Jones matrices*. Based on this formalism, the operation performed on the light by each component in spectroscopic ellipsometry, such as the polarizer, analyzer, and compensator, can be represented as a 2×2 matrix operator.

For instance, in the case of a linear polarizer with the azimuthal angle, α, relative to the x–y coordinates of a linearly polarized light, E_i, the process of linear polarization can be expressed as

$$E_f = \begin{bmatrix} \cos\alpha & 0 \\ 0 & \sin\alpha \end{bmatrix} \tag{1.15}$$

Transformations by a series of optical components can be represented by the corresponding series of matrix operations.

While the Jones vector is a concise way for describing polarized light, it is unable to express unpolarized light and light that is partially polarized. Therefore, the *Stokes parameters* (vectors) are used for the description of lights with different polarization [4].

The components of the Stokes vector are

$$\mathbf{S}_0 = I_x + I_y = E_x E_x^* + E_y E_y^* \tag{1.16a}$$

$$\mathbf{S}_1 = I_x - I_y = E_x E_x^* - E_y E_y^* \tag{1.16b}$$

$$\mathbf{S}_2 = I_{+45^\circ} + I_{-45^\circ} = 2E_{x_0} E_{y_0} \cos\Delta \tag{1.16c}$$

$$\mathbf{S}_3 = I_\mathrm{R} - I_\mathrm{L} = -2E_{x_0} E_{y_0} \sin\Delta \tag{1.16d}$$

where I_x and I_y denote the intensities of the linearly polarization light along the x- and y-axes, respectively. Likewise, $I_{\pm 45^\circ}$ represents light polarization $\pm 45^\circ$ to the x-axis, while $I_\mathrm{L}/I_\mathrm{R}$ represent intensities of left-/right-circularly polarized light. Finally, $\Delta = \delta_x - \delta_y$.

The Stokes vector can also be expressed as

$$\mathbf{S} = \begin{bmatrix} \mathbf{S}_0 \\ \mathbf{S}_1 \\ \mathbf{S}_2 \\ \mathbf{S}_3 \end{bmatrix} \tag{1.17}$$

Transformation of a Stokes vector can be expressed via a 4×4 matrix representation, also known as a *Mueller matrix*. The calculation is performed in a fashion similar to the Jones matrix. For instance, when linear polarization oriented at 45° passes a polarizer with transmission axis along the x-direction, the resultant light that emerges from the polarizer is transformed via the following:

$$\frac{1}{2}\begin{pmatrix} 1 & 1 & 0 & 0 \\ 1 & 1 & 0 & 0 \\ 0 & 0 & 0 & 0 \\ 0 & 0 & 0 & 0 \end{pmatrix}\begin{pmatrix} 1 \\ 0 \\ 1 \\ 0 \end{pmatrix} = \begin{pmatrix} 1/2 \\ 1/2 \\ 0 \\ 0 \end{pmatrix} \tag{1.18}$$

1.2 Principles of Ellipsometric Measurements

When light is reflected/transmitted from a sample, the p- and s-polarized components of the incident light undergo changes to their amplitude and phase. Hence, spectroscopic ellipsometry is a technique that capitalizes on these changes where the essential optical parameters are derived. As mentioned, the raw quantities measured using ellipsometry are Ψ and Δ, representing the amplitude ratio and phase difference between reflected or transmitted p- and s-polarized waves, respectively. These two quantities are related complex reflection coefficients via the expression

$$\varrho \equiv \tan\Psi \exp i\Delta = \frac{r_\mathrm{p}}{r_\mathrm{s}} \tag{1.19}$$

with r_p and r_s defined as ratios of the light reflected to the incident E-fields.

Equation (1.19) can be further expressed as

$$\tan\Psi \exp i\Delta = \frac{r_{\mathrm{p}}}{r_{\mathrm{s}}} = \frac{E_{rp}/E_{ip}}{E_{rs}/E_{is}} = E_{rp}/E_{rs} \tag{1.20}$$

where the final step of simplification can be performed since $E_{\mathrm{ip}} = E_{\mathrm{is}}$.

Different spectroscopic ellipsometry setups are available, of which the raw Ψ and Δ are measured by different means. Generally, the systems are classified into two main categories – spectroscopic ellipsometers with rotating optical elements and those with photoelastic modulators. In our study, focus will be on the system with rotating optical elements (i.e. rotating analyzer with compensator). The working principle of such spectroscopic ellipsometers will be described briefly in Section 1.2.1.

1.2.1 Rotating-Analyzer Ellipsometer

A rotating-analyzer spectroscopic ellipsometer (Figure 1.1) is one of the few ellipsometric setups that is widely used. The changes made to an incident light wave when passing through a rotating-analyzer spectroscopic ellipsometer can be represented as a series of matrix operations $\mathrm{PSA_R}$, where P, S, and $\mathrm{A_R}$ denote the polarizer, the sample, and the rotating analyzer, respectively. In spectroscopic ellipsometry, the wavelength of the incident photon is typically changed using a monochromator. However, this slows down the operational speed of the system. Hence, in many spectroscopic ellipsometry systems, especially those for real-time monitoring, a grating spectrometer is typically used in the detector probe, while white light is used as the incident source.

By applying the Jones vectors and Mueller matrices, the output of the $\mathrm{PSA_R}$ ellipsometric configuration can be expressed as

$$L_{\mathrm{out}} = \mathrm{AR}(A)R(-P)PL_{\mathrm{in}} \tag{1.21}$$

where the Jones vector of the light wave at the detector can be expressed as $L_{\mathrm{out}} = \begin{bmatrix} E_A \\ 0 \end{bmatrix}$. $L_{\mathrm{in}} = \begin{bmatrix} 1 \\ 0 \end{bmatrix}$ denotes the input Jones vector of the incident light source. $R(A)$ represents the rotation matrix with a rotation angle of the analyzer at A. P denotes the rotation angle of the polarizer and S represents the Jones matrix corresponding to the reflected light off the sample.

Hence, Eq. (1.21) is expressed in the matrix form as

$$\begin{bmatrix} E_A \\ 0 \end{bmatrix} = \begin{bmatrix} 1 & 0 \\ 0 & 0 \end{bmatrix} \begin{bmatrix} \cos A & \sin A \\ -\sin A & \cos A \end{bmatrix} \begin{bmatrix} \sin\Psi \exp i\Delta & 0 \\ 0 & \cos\Psi \end{bmatrix} \begin{bmatrix} \cos P & -\sin P \\ \sin P & \cos P \end{bmatrix} \begin{bmatrix} 1 & 0 \\ 0 & 0 \end{bmatrix} \begin{bmatrix} 1 \\ 0 \end{bmatrix}$$

If polarization angle $P = 45°$, it will then take the form

$$\begin{bmatrix} E_A \\ 0 \end{bmatrix} = \begin{bmatrix} 1 & 0 \\ 0 & 0 \end{bmatrix} \begin{bmatrix} \cos A & \sin A \\ -\sin A & \cos A \end{bmatrix} \begin{bmatrix} \sin\Psi \exp i\Delta \\ \cos\Psi \end{bmatrix} \tag{1.22}$$

which ultimately leads to the solution

$$E_A = \cos A \sin\Psi \exp i\Delta + \sin A \cos\Psi \tag{1.23}$$

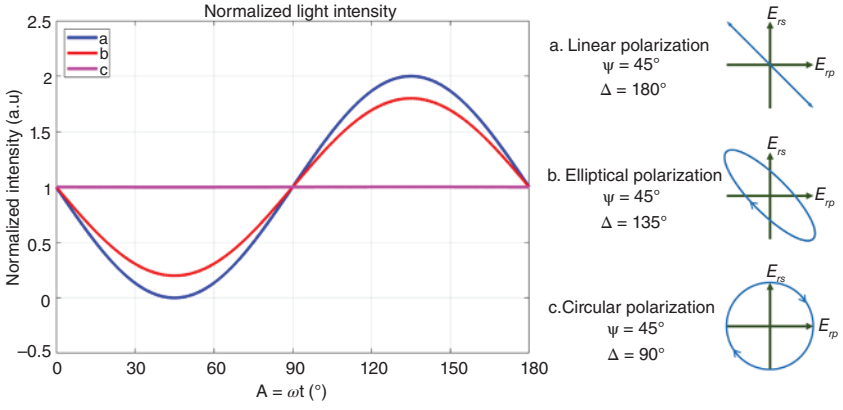

Figure 1.3 Normalized intensity of linearly, elliptical, and circularly polarized light based on the rotating-analyzer configuration.

The light intensity registered at the detector can then be expressed as the modulus square of E_A:

$$\begin{aligned} I &= |E_A|^2 \\ &= I_0(1 - \cos 2\Psi \cos 2A + \sin 2\Psi \cos \Delta \sin 2A) \\ &= I_0(1 + S_1 \cos 2A + S_2 \sin 2A) \end{aligned} \tag{1.24}$$

where I_0 represents the proportionality constant of the reflected light. The period of the intensity variation is π radians (180°). Generally, the Stokes parameters, S_1 and S_2, in a rotating-analyzer ellipsometer (RAE) are measured as Fourier coefficients of cos $2A$ and sin $2A$, respectively. When the analyzer rotates at an angular frequency of ω, the general expression of the detector intensity is expressed as

$$I(t) = I_0(1 + \alpha \cos 2\omega t + \beta \sin 2\omega t) \tag{1.25}$$

where the normalized intensity registered at the detector based on Eq. (1.25) is plotted in Figure 1.3.

1.3 Experimental Setup

The spot size of the beam is in the range of 3–5 mm with additional detachable microfocus, which can be used to focus the spot size to an even smaller dimension of about 200 μm. Such a small beam spot is suitable for the optical characterization of smaller samples to reduce the instances of back reflection and scattering in transparent samples.

The input unit consists of a lens mount, a polarizer stage, and an alignment detector socket. Polarization state of the light beam is detected before its incidence on the sample, which is mounted on the sample stage. After reflecting off the sample surface, the detector unit converts the reflected beam into a voltage and measures

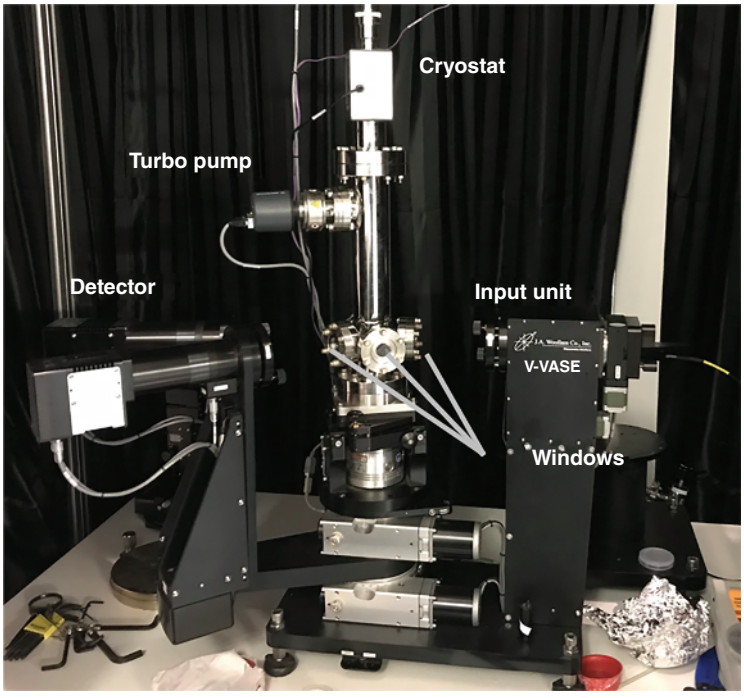

Figure 1.4 Woollam VASE spectroscopic ellipsometer.

its polarization state. The software (WVASE32) is then used to analyze the raw data from which the optical parameters of the sample are derived.

1.3.1 VASE Spectroscopic Ellipsometer

The setup of the Variable-Angle Spectroscopic Ellipsometer (VASE) by J. A. Woollam Co., Inc. is displayed in Figure 1.4. The arc lamp provides a broadband light source for the HS-190 monochromator (Czerny–Turner Scanning Monochromator), which the software uses to supply a selected wavelength/photon energy of light for the system. This spectroscopic ellipsometer provides both high accuracy and precision along with a wide spectral range of ~190–2500 nm (~0.5–6.5 eV), covering the near-IR, visible, and near-UV regimes. With this broad spectral range, this system is suitable for characterizing optical bandgaps and electronic transitions for semiconducting and Mott-insulating systems (Figure 1.5).

RAE of the VASE spectroscopic ellipsometer helps to maximize data accuracy near the "Brewster" angle [1], where the raw Ψ and Δ data are content-rich. The autoretarder is a computer-controlled waveplate that modifies the beam polarization (from linear to circular polarization or vice versa) before reaching the sample. This process provides greater accuracy for the measurement of the Δ parameter even when the phase difference is close to the extremum angles of 0° and 180°. This process produces optimum measurement conditions for the sample.

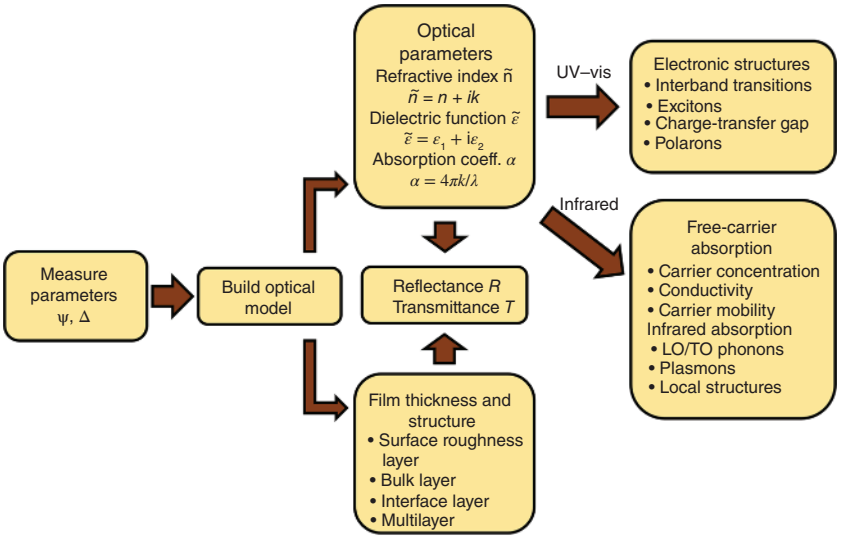

Figure 1.5 Characteristic properties of spectroscopic ellipsometry and the electronic features that it can detect in the respective spectral region. Source: Adapted from Fujiwara [5].

1.3.2 IR-VASE Spectroscopic Ellipsometer

The J. A. Woollam IR-VASE has a spectral range of ~1.7–30 μm (near the far-infrared regime), and it can measure spectroscopic ellipsometry data in both the reflection and the transmission modes. Having both the chemical sensitivity of Fourier transform infrared (FTIR) spectroscopy and precise thin-film sensitivity, this device is suitable for the characterization of both thin-film and bulk material systems. Apart from characterizing sample parameters, such as film thickness and dielectric functions that are typical of spectroscopic ellipsometry, the spectral range within which IR-VASE falls is also capable of characterizing unique features, such as chemical bonding (molecular vibrations) and phonon absorption in crystalline systems (Figure 1.5).

IR-VASE integrates a FTIR interferometer source with a rotating compensator ellipsometer to provide accurate spectroscopic ellipsometry measurements. It combines a broadband polarizer and a compensator with an optimized beam splitter, collimators, and a deuterated triglycine sulfate (DTGS) detector, which in turn provides a very wide spectral range.

During the measurement process, the compensator is rotated by 360° in a series of steps. This intensity spectrum is the outcome of the sample optical and polarization properties along with the effects of the compensator and polarizers. The Ψ and Δ spectra (and other sample quantities) are then calculated based on the combination of the intensity spectra from each position of the compensator.

Table 1.1 Advantages and disadvantages of spectroscopic ellipsometry.

Advantages	Nondestructive
	High precision
	Fast measurement
	Multiple characterization (e.g. optical properties and film thickness)
	Real-time monitoring
Disadvantages	Complicated data analysis
	Require large, full-covered sample (at least $\sim 3 \times 3\ mm^2$)
	Difficulty to characterize materials with low absorption coefficients
	Indirect characterization – optical model required
	Sample surface roughness must be small
	Measurements to be performed at oblique angles

Source: Modified from Fujiwara [5].

1.4 Spectroscopic Ellipsometry: General Profiles

Spectroscopic ellipsometry has a broad range of applications. In terms of real-time application, not only does it allow for the real-time monitoring of thin-film growth, but also process diagnoses, such as the tracking of etching and thermal oxidation, can be carried out [6]. However, the surface roughness of the sample must be small and optical characterization has to be performed at oblique incident angles. This is because reflected light intensity can be severely impaired by surface roughness, which in turn makes it difficult for ellipsometry measurements, particularly due to the characterization of the polarization state from the light intensity. The measurement errors increase in correspondence with the magnitude of sample surface roughness [5].

Table 1.1 provides a comprehensive summary of the advantages and disadvantages of spectroscopic ellipsometry as an experimental technique. Two important features of spectroscopic ellipsometry are its high measurement precision and thickness sensitivity ($\sim$1 Å) [5]. These crucial features make it an indispensable instrument for the precise optical characterization and morphological analysis of thin-film structures. This will be illustrated in Chapters 3 and 4 where the optical characterization of 2D-TMDs whose thickness is in the order of $\sim$2 nm and below [7].

However, with the indirect characterization of the ellipsometry data, data analysis is difficult when the optical profiles and sample structures (e.g. sample thickness) are unclear. This is because data analysis requires an optical model that includes the optical parameters and sample film thickness. These factors complicate the analytical process to elucidate the sample optical data [8].

1.5 Ellipsometric Data for Multilayered System

The measured quantities Ψ and Δ in spectroscopic ellipsometry are the amplitude ratio and phase difference between the p- and s-polarized light reflected/transmitted off a surface, respectively. These two quantities are related via Eq. (1.19) as mentioned in Section 1.2 with Figure 1.6 illustrating the optical interference in an ambient/film/substrate system.

A commonly used sample system for consideration is the ambient/film/substrate structure. In this case, the amplitude reflection coefficients are expressed as

$$r_{012,\mathrm{p}} = \frac{r_{01,\mathrm{p}} + r_{12,\mathrm{p}} \exp -i2\beta}{1 + r_{01,\mathrm{p}} \cdot r_{12,\mathrm{p}} \exp -i2\beta} \tag{1.26a}$$

$$r_{012,\mathrm{s}} = \frac{r_{01,\mathrm{s}} + r_{12,\mathrm{s}} \exp -i2\beta}{1 + r_{01,\mathrm{s}} \cdot r_{12,\mathrm{s}} \exp -i2\beta} \tag{1.26b}$$

while the transmission coefficients are expressed as

$$t_{012,\mathrm{p}} = \frac{t_{01,\mathrm{p}} + t_{12,\mathrm{p}} \exp -i\beta}{1 + r_{01,\mathrm{p}} \cdot r_{12,\mathrm{p}} \exp -i2\beta} \tag{1.27a}$$

$$t_{012,\mathrm{s}} = \frac{t_{01,\mathrm{s}} + t_{12,\mathrm{s}} \exp -i\beta}{1 + r_{01,\mathrm{s}} \cdot r_{12,\mathrm{s}} \exp -i2\beta} \tag{1.27b}$$

The film thickness, d, is related to the phase thickness, β, via the following relation:

$$\beta = 2\pi d N_1 \cos(\theta_1 / \lambda) \tag{1.28}$$

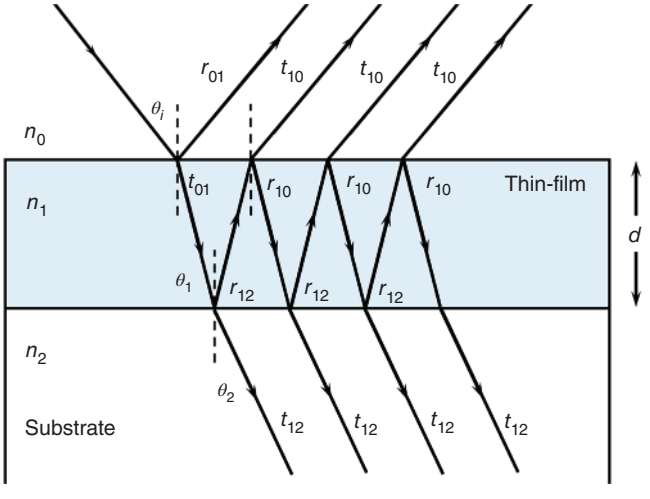

Figure 1.6 Optical model for an ambient/film/substrate system.

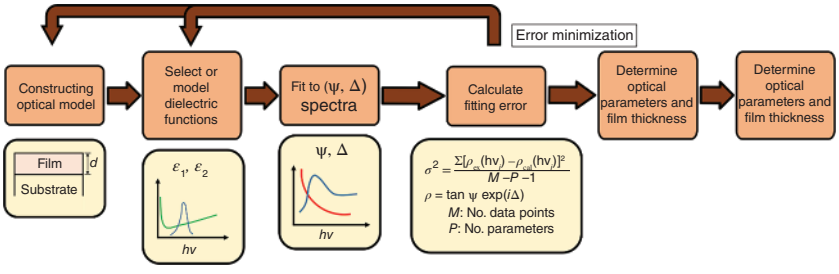

Figure 1.7 Flowchart of the data analysis procedure in spectroscopic ellipsometry.

Therefore, the fundamental ellipsometric equation can be expanded from Eq. (1.19) into the following:

$$\tan\Psi \exp i\Delta = \frac{r_p}{r_s} = \left[\frac{r_{01,p} + r_{12,p}\exp -i2\beta}{1 + r_{01,p}\cdot r_{12,p}\exp -i2\beta}\right] / \left[\frac{r_{01,s} + r_{12,s}\exp -i2\beta}{1 + r_{01,s}\cdot r_{12,s}\exp -i2\beta}\right] \quad (1.29)$$

Procedures to extract the relevant optical parameters are carried out in four main steps (Figure 1.7). Firstly, spectroscopic ellipsometry measurements yield reflected/transmitted light intensity ratio (tan Ψ) and phase difference (exp $i\Delta$) between the respective polarization states. By constructing a sample model based on the actual sample structure and fitting the raw experimental data (Ψ, Δ) to the model, the exact optical parameters such as the dielectric function, optical conductivity, and/or sample thickness are eventually derived.

Model selection is the most vital and complex segment of the fitting procedure in the derivation of the optical parameters. Two key methods can be employed for modeling and fitting analysis – the commonly employed parameterized or oscillator model and the wavelength-by-wavelength best-match model.

1.6 Dielectric Models

Characterization of materials using spectroscopic ellipsometry allows the possibility of fitting the optical response data to physical models. These models describe the dynamics of charge carriers (e.g. electrons) in a system. The *Drude model* of electrical conduction models a system as a charged carrier (electron) gas executing a diffusive motion in the presence of positively charged ionic cores [9, 10]. They are effectively free electrons not bound by any positively charged ions in the system. Hence, the Drude model is mainly used to describe the transport properties of electrons in metallic or doped semiconducting systems.

As for dielectric materials, several types of oscillations may occur when perturbed by an external electromagnetic field. This includes bound electron oscillations and phonon vibrations [11]. The *Lorentz model* is employed to model the optical responses of such systems when subject to external electromagnetic radiation.

It is commonly used to study the optical properties of band semiconductors and insulators [9].

For more general cases such as doped semiconductors where both insulating and conducting properties are present, the collective model known as the *Drude–Lorentz model* can be used to model such systems that contain both free and oscillating charged carriers.

1.6.1 Drude Model

Several assumptions have been made in consideration of this model.

1. Electrons in the system are considered free electrons. No interaction between the electrons takes place during the interval between collisions.
2. Electron collisions occur at an average of once every time τ, where τ is known as the average relaxation time and its inverse, τ^{-1}, is known as the scattering rate, γ.
3. Electrons only achieve thermal equilibrium with the surroundings through collisions [10].
4. Long-range interaction between the electrons and the ions is neglected. Besides, there is no interaction between electrons. The only form of interaction is the instantaneous collision between an electron and an ion. The instantaneous collision results in the change of electron velocity.

In the absence of an external electric field $\vec{E}$, the mean electron momentum $\langle\vec{p}\rangle = 0$ and the rate equation of the mean electron momentum $\langle\vec{p}\rangle$ can be expressed as

$$\frac{d\langle\vec{p}\rangle}{dt} = -\frac{\langle\vec{p}\rangle}{\tau} \tag{1.30}$$

In this case, assumptions 2 and 3 come into play, such that the average relaxation time, τ, determines the relaxation of the system to equilibrium [9]. In the presence of the external electric field, $\vec{E}$, Eq. (1.30) takes the form

$$\frac{d\langle\vec{p}\rangle}{dt} = -\frac{\langle\vec{p}\rangle}{\tau} - \mathrm{e}\vec{E} \tag{1.31}$$

where −e denotes the electronic charge.

The current density due to the electrons is

$$\vec{J} = -n\mathrm{e}\langle\vec{v}\rangle = -\frac{n\mathrm{e}}{m_\mathrm{e}}\langle\vec{p}\rangle \tag{1.32}$$

where n denotes the charge density, m_e the electron mass, and $\langle\vec{v}\rangle$ the mean electron velocity.

The case of a constant $\vec{E}$ field (i.e. dc fields), $\frac{d\langle\vec{p}\rangle}{dt} = 0$, results in dc conductivity,

$$\sigma_\mathrm{dc} = \vec{J}/\vec{E} = n\mathrm{e}^2\tau/m_\mathrm{e} \tag{1.33}$$

In the case of an oscillating $\vec{E}$-field in the form $\vec{E}(t) = \vec{E}_0 \exp -i\omega t$, Eq. (1.31) can be expressed in the form of a second-order differential equation:

$$m_\mathrm{e}\frac{d^2\vec{r}}{d^2t} + \frac{m_\mathrm{e}}{\tau}\frac{d\vec{r}}{dt} + \mathrm{e}\vec{E}(t) = 0 \tag{1.34}$$

whose solution yields a frequency-dependent complex conductivity in the form [9]

$$\widetilde{\sigma}(\omega) = \frac{ne^2\tau}{m_e}\frac{1}{1-i\omega\tau} \tag{1.35}$$

Here, we define a new parameter known as the *plasma frequency*:

$$\omega_p = \sqrt{(ne^2/\varepsilon_0 m_e)} \tag{1.36}$$

The plasma frequency, ω_p, is proportional to the square root of the electron density over its mass. More generally, $\omega_p \propto \sqrt{(n/m^*)}$, where n refers to the general charged carrier density, while m^* denotes the effective mass of the charged carriers. Hence, Eq. (1.35) can be re-expressed in the form

$$\widetilde{\sigma}(\omega) = \frac{\varepsilon_0\omega_p^2}{1/\tau - i\omega} \tag{1.37}$$

where the real and imaginary components are resolved into the following:

$$\sigma_1(\omega) = \frac{\varepsilon_0\omega_p^2\tau}{1+\omega^2\tau^2} \tag{1.38a}$$

$$\sigma_2(\omega) = \frac{\varepsilon_0\omega_p^2\omega\tau^2}{1+\omega^2\tau^2} \tag{1.38b}$$

When expressed in terms of dielectric function, Eq. (1.37) takes the form

$$\widetilde{\varepsilon}(\omega) = 1 - \frac{\omega_p^2}{\omega^2 - \frac{i\omega}{\tau}} \tag{1.39}$$

which can be further resolved into its respective components:

$$\varepsilon_1(\omega) = 1 - \frac{\omega_p^2\tau}{\omega^2 + 1/\tau^2} \tag{1.40a}$$

$$\varepsilon_2(\omega) = \frac{1}{\omega\tau}\frac{\omega_p^2}{\omega^2 + 1/\tau^2} \tag{1.40b}$$

The frequency-dependent dielectric function, $\widetilde{\varepsilon}(\omega)$, modeled typically for good metals based on the Drude model Eqs. (1.40a) and (1.40b) is depicted in Figure 1.8.

1.6.2 Lorentz Model

Extension was made to The Drude model, named after Paul Drude in 1900, was extended and further modified to account for quantum phenomena years [12]. A notable extension to the Drude model is known as the *Lorentz model* in the study of optical properties in semiconductors and insulators. In the Lorentz oscillator model, electrons are bound to a nucleus with a resonant frequency of ω_0. This is modeled after the classical model of electrons bound to a heavy nucleus by springs, which results in an atomic oscillatory motion with natural frequencies $\omega_0 = \sqrt{K/\mu}$ (Figure 1.9). Here, K denotes the spring constant, while μ, the reduced mass of the oscillatory system, is expressed as

$$1/\mu = 1/m_n + 1/m_e \tag{1.41}$$

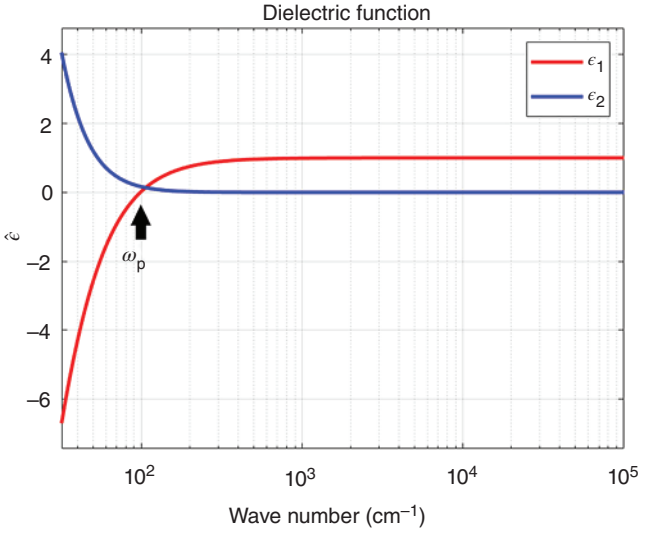

Figure 1.8 Dielectric function, $\widetilde{\varepsilon}$, of a Drude system plotted with respect to wave number in semi-logarithmic scale where plasma frequency $\omega_p = 10^4$ cm^{-1} and scattering rate $\gamma = 1/\tau = 17$ cm^{-1}. Note that the zero-crossing for ε_1 takes place at the plasma frequency as annotated in the figure.

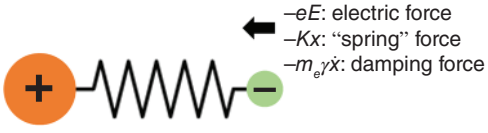

Figure 1.9 Oscillatory system to illustrate the Lorentz model.

where m_n and m_e denote the nuclear and electron mass, respectively.

Such resonant frequencies are now known to correspond to the quantized transition energy [11] of the quantum harmonic oscillator. Since it can be assumed that $m_n \gg m_e$, the approximation $\mu \approx m_e$ can be made. Dynamics of the oscillatory electron can be modeled after a damped harmonic oscillator system where the damping process occurs due to energy lost due to particle collisions. Hence, the Lorentz model can be expressed as a second-order differential equation:

$$m_e \frac{d^2\vec{r}}{dt^2} + \frac{m_e}{\tau}\frac{d\vec{r}}{dt} + m_e\omega_0^2\vec{r} = -e\vec{E}(t) \tag{1.42}$$

where the damping effect is taken into consideration by the parameter τ. $\vec{E}(t) \propto \exp -i\omega t$ represents the time-dependent electric field of the incident electromagnetic wave.

A solution to the differential Eq. (1.42) is [9]

$$\vec{r}(\omega) = -\frac{\frac{e\vec{E}}{m_e}}{\left(\omega_0^2 - \omega^2\right) - \frac{i\omega}{\tau}} \tag{1.43}$$

The optical conductivity modeled after the Lorentz model can be derived and expressed as

$$\widetilde{\sigma}(\omega) = \frac{ne^2}{m_e} \frac{\omega}{i\left(\omega_0^2 - \omega^2\right) + \omega/\tau} = \varepsilon_0 \frac{\omega_p^2 \omega}{i\left(\omega_0^2 - \omega^2\right) + \omega/\tau} \tag{1.44}$$

where the plasma frequency $\omega_p = \sqrt{(ne^2/\varepsilon_0 m_e)}$.

The respective components of Eq. (1.44) are

$$\sigma_1(\omega) = \varepsilon_0 \frac{\omega_p^2 \omega^2/\tau}{\left(\omega_0^2 - \omega^2\right)^2 + \omega^2/\tau^2} \tag{1.45a}$$

$$\sigma_2(\omega) = -\varepsilon_0 \frac{\omega_p^2 \omega \left(\omega_0^2 - \omega^2\right)}{\left(\omega_0^2 - \omega^2\right)^2 + \omega^2/\tau^2} \tag{1.45b}$$

In terms of dielectric function, Eq. (1.44) takes the form

$$\widetilde{\varepsilon}(\omega) = 1 + \frac{\omega_p^2}{\left(\omega_0^2 - \omega^2\right) - i\omega/\tau} \tag{1.46}$$

with the respective components as

$$\varepsilon_1(\omega) = 1 + \frac{\omega_p^2 \left(\omega_0^2 - \omega^2\right)}{\left(\omega_0^2 - \omega^2\right)^2 + \omega^2/\tau^2} \tag{1.47a}$$

$$\varepsilon_2(\omega) = \frac{\omega_p^2 \omega/\tau}{\left(\omega_0^2 - \omega^2\right)^2 + \omega^2/\tau^2} \tag{1.47b}$$

with Figure 1.10 displaying the dielectric profiles akin to a narrow-gap semiconductor. It can be seen from Eq. (1.46) that by setting the resonant frequency $\omega_0 = 0$, Eq. (1.39) belonging to the Drude model can be derived.

Generally, there are multiple bound electron oscillators in a dielectric material. Hence, the optical conductivity according to the Lorentz model is expressed in a general form as

$$\widetilde{\sigma}(\omega) = \sum_k \varepsilon_0 \frac{\omega_{pk}^2 \omega}{i\left(\omega_{0k}^2 - \omega^2\right) + \omega/\tau_k} \tag{1.48}$$

to sum up the contributions to the optical conductivity by multiple dipole oscillators.

Notice that a resonance peak occurs at $\omega_0 (= \omega/2\pi c)$. $1/\tau$ denotes the peak broadening due to damping and plasma frequency and ω_p may be understood as the oscillator strength [9].

1.6.3 Drude–Lorentz Model

When the system has both metallic and semiconducting properties, both the Drude and the Lorentz components can be included in the model. In this case, while the electrons in the system are unbound, there is a spring-like interactive force with the positively charged nuclei. The dielectric functions that comprise both the Drude and Lorentz components are depicted in Figure 1.11.

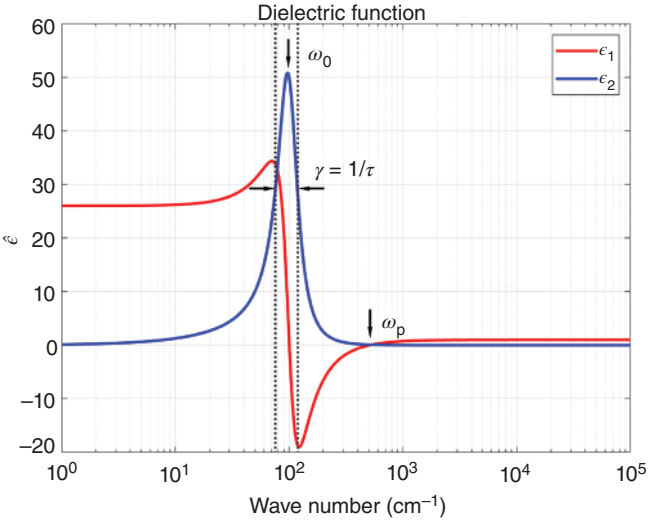

Figure 1.10 Dielectric function $\widetilde{\varepsilon}$ of a Lorentz oscillator plotted with a semilogarithmic scale with the respective profiles indicated [9].

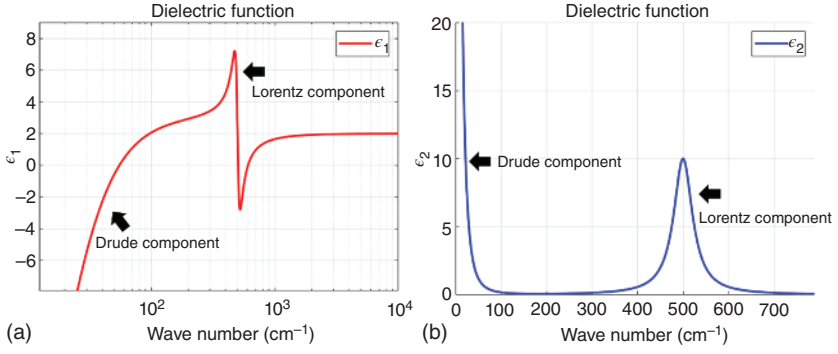

Figure 1.11 (a) ε_1 and (b) ε_2 components based on the Drude–Lorentz model with both metallic and semiconducting properties.

1.6.4 Sellmeier and Cauchy Models

In the case of large-bandgap insulating samples with a simple band structure at the pre-edge (where $\varepsilon_2 \approx 0$) [5], the Lorentz oscillator model equation can be rewritten as the Sellmeier equation where $\omega \ll \omega_{[0,j]}$.

As a function of wavelength, λ, the expression is given as

$$\varepsilon(\lambda) = A + \sum_k \frac{B_k \lambda^2}{\lambda^2 - \lambda_{0,k}^2} \tag{1.49}$$

where $\lambda_{[0,k]}$ denotes the peak position of the jth oscillator. The Sellmeier Eq. (1.49) can be further expanded to the Cauchy form to simplify the data analysis [5]

$$\widetilde{n}(\lambda) = A + \frac{B}{\lambda^2} + \frac{C}{\lambda^4} + \cdots \tag{1.50}$$

1.7 Chapter Summary

This chapter has provided sufficient experimental and theoretical groundwork for the analysis and discussion of experimental data obtained via spectroscopic ellipsometry. Readers have been given a basic understanding of the inner workings of spectroscopic ellipsometry. In addition, the Drude, Lorentz, and other related optical models have been introduced. These will be essential in the study of the optical responses of metallic and semiconducting materials. The Drude–Lorentz model has been discussed for the analysis of materials comprising both metallic and dielectric properties. This will help in the understanding and analysis of the 2D quantum systems as presented in Chapters 3 and 4.

References

1 Jackson, J.D. (1998). *Classical Electrodynamics*, *3*e. John Wiley & Sons, Inc.
2 Armitage, N.P., Fournier, P., and Greene, R.L. (2010). Progress and perspectives on electron-doped cuprates. *Reviews of Modern Physics* 82: 2421–2487, https://doi.org/10.1103/RevModPhys.82.2421.
3 Homes, C.C., Timusk, T., Liang, R. et al. (1993). Optical conductivity of *c* axis oriented $YBa_2Cu_3O_{6.70}$: evidence for a pseudogap. *Physical Review Letters* 71: 1645–1648, https://doi.org/10.1103/PhysRevLett.71.1645.
4 Collett, E. (2005). *Field Guide to Polarization*. SPIE Press.
5 Fujiwara, H. (2007). *Spectroscopic Ellipsometry: Principles and Applications*. John Wiley & Sons, Inc.
6 An, I., Li, Y.M., Nguyen, H.V., and Collins, R.W. (1992). Spectroscopic ellipsometry on the millisecond time scale for real-time investigations of thin-film and surface phenomena. *Review of Scientific Instruments* 63: 3842–3848, https://doi.org/10.1063/1.1143280.
7 Tompkins, H.G. and Haber, E.A. (2005). *Handbook of Ellipsometry*. William Andrew Publishing.
8 Tompkins, H.G. and Hilfiker, J.N. (2016). *Spectroscopic Ellipsometry: Practical Application to Thin Film Characterization*. Momentum Press.
9 Dressel, M. and Gruner, G. (2002). *Electrodynamics of Solids: Optical Properties of Electrons in Matter*. Cambridge University Press.
10 Singleton, J. (2001). *Band Theory and Electronic Properties of Solids*. Oxford University Press.
11 Fox, M. (2002). *Optical Properties of Solids*, *2*e. Oxford University Press.
12 Drude, P. (1900). Zur Elektronentheorie der Metalle. *Annalen der Physik* 306: 566–613, https://doi.org/10.1002/andp.19003060312.